NASA Technical Memorandum 87773



# Objective Analysis of Tidal Fields in the Atlantic and Indian Oceans

Braulio V. Sanchez, Desiraju B. Rao,
and Stephen D. Steenrod

JUNE 1986



NASA

NASA Technical Memorandum 87773

# Objective Analysis of Tidal Fields in the Atlantic and Indian Oceans

Braulio V. Sanchez
*Goddard Space Flight Center*
*Greenbelt, Maryland*

Desiraju B. Rao
*National Meteorological Center*
*National Oceanic and Atmospheric Administration*
*Washington, D.C.*

Stephen D. Steenrod
*Applied Research Corporation*
*Landover, Maryland*

National Aeronautics
and Space Administration

**Scientific and Technical
Information Branch**

**1986**

# 1. INTRODUCTION

The accurate modeling of oceanic tides is very important for the interpretation of oceanic measurements from space borne altimeters. The tides not only introduce errors into the determination of geostrophic velocity but they are of considerable interest in their own right. Tidal investigations of ocean basins with realistic topography and coastal boundaries are still in the developing stage.

Ocean tidal studies have a long history. Several comprehensive reviews can be found in the literature, i.e., Hendershott and Munk (1970), Cartwright (1977), Hendershott (1973, 1977, 1981) and Schwiderski (1980).

Hendershott (1977) summarized the efforts to solve the LTE for global tides for semidiurnal and diurnal components up to that time. The majority of the M2 calculations agree in the prediction of both a North and a South Atlantic amphidrome, although they vary widely in the resolution and prediction of coastal tides and none is able to resolve the tides over the shallow Patagonian shelf. An anti-amphidrome is predicted consistently in the central Indian ocean with the coastal details showing wide variation for the different models. In the southeast Pacific some calculations yield a confluence of cotidal lines with low amplitude while other models locate an amphidrome there. No data are available to resolve the discrepancy. The northwest Pacific is different in every model.

More recent efforts have been directed to incorporate the results of loading and self-attraction. Accad and Pekeris (1978) solve the Laplace's tidal equations for the M2 and S2 tides in the world oceans on the basis of a knowledge of the tidal potential alone. Tidal dissipation was taken to be limited to the coastline. The main purpose of their investigation was to determine the effects of tidal self-attraction and of tidal loading. An iterative method was developed to evaluate these secondary effects, the resulting change is of the order of 10% and better agreement is obtained between the theoretical and observed tides. Parke and Hendershott (1980) obtained global solutions to the Laplace's tidal equations for the M2, S2 and K1 tides. They addressed the problem of divergence of the near-resonance modes by means of test functions which are used to interpolate between island data in the least squares sense. These test functions are derived by solving Laplace's tidal equations with ocean loading and selfgravitation in an iterative manner. The resulting representations of the global tide are stable over at least a $\pm 5\%$ variation in the mean depth of the model basin and they conserve mass.

Schwiderski (1980) computed the M2 global tide by solving the Laplace's tidal equations directly, using a finite difference scheme in space and time; the strictly mathematical solution was modified by means of an interpolation technique which incorporates over 2000 tide data collected at continental and island stations, the interpolation is accomplished by adjusting the bottom friction coefficient and by allowing in or out-flow across the mathematical ocean boundary. No direct comparison of observed and computed data is feasible since the model incorporates essentially all known data although it is possible to evaluate the smoothness with which the computed tide accepts or rejects data. It was found that the interpolation technique permits a check of the reality of both the tide model and the tidal data input.

Platzman (1978,1981,1984) has computed a range of normal modes for the world oceans. He used them to synthesize some of the diurnal and semidiurnal tides. He decomposed the transport vector by means of the Stokes/Helmholtz potentials but did not determine the velocity potential and stream function eigenfunctions explicitly (as in this paper), but proceeded directly to the normal mode solution of the L.T.E. The linearized primitive equations were discretized by means of first-order, piecewise-linear finite elements with an average grid triangle area equal to that of a 4.54° equatorial square. His synthesized tides incorporated dissipation by means of energy flux across the domain boundary and no tidal loading or self attraction was included.

The numerical ocean tidal models currently available differ by several tens-of-centimeters in many areas of the world. The precision altimetric measurements of the sea surface topography now provide the capability of independently assessing the accuracy of these models. Simulation studies by Estes (1980) using numerical

solutions of the Laplace's tidal equations to generate the observed measurements (based on simulated 4-day SEASAT orbits over a 200-day interval) indicate that when the rms amplitude error is less than 10 cm for the M2 tide virtually all the structure is recovered. For rms errors between 12 and 15 cm all large scale features are retained, for 15 cm to 20 cm rms errors the high amplitude structure is recovered. These results were obtained by utilizing long arc intersection, or crossover point data and simultaneously solving for the orbit error parameters with the tide model parameters.

Mazzega (1985) created a global model of the M2 tide using twenty four days of SEASAT altimetry data, the solution was obtained by means of surface spherical harmonics, the results were qualitatively realistic. No hydrodynamic equations were used.

The purpose of this investigation is to develop an objective analysis technique which will serve to extrapolate tidal amplitudes and phases over entire ocean basins using existing gauge data and the precise altimetric measurements which are now beginning to be provided by satellite oceanography. The applicability of the extrapolating technique was tested in the Lake Superior basin by Sanchez, Rao and Wolfson (1985). Proceeding in stages we now report the results obtained in the Atlantic-Indian oceans using a $6° \times 6°$ grid. At this level of resolution it is possible to test the essential features of the method without using real data.

The method to be used in this investigation requires several distinct steps. First it is necessary to determine numerically the stream function and velocity potential orthogonal functions (The Stokes/Helmholtz Potentials) which span the space of the basin under consideration. These space functions are then used in the Laplace tidal equations to determine the homogeneous solution (normal modes) and the forced solution. The latter is obtained by adding the astronomical forcing function modified to include solid-earth tides.

The velocity potential eigenfunctions obtained as a first step are used also to extrapolate the surface height field over the entire space domain of the given basin and this approach will constitute a distinct and integral part of the investigation.

The theoretical foundation is Proudman's theory (1918) as formulated by Rao (1966). The theory provides the formalism for calculation of the gravitational (first class) normal modes and the rotational (second class or Rossby waves) normal models of irregularly shaped basins with realistic bathymetry.

The method requires the solution of two elliptic partial differential equations with second order operators which are simpler than the tidal operator. The boundary conditions correspond to vanishing of the stream function and normal derivative of the velocity potential. The elliptic operators are represented numerically in finite difference form, the grid used is a Richardson lattice which preserves self-adjointness. The solutions yield the velocity and surface height fields in terms of orthogonal functions with time-dependent coefficients. These functions are then substituted into the Laplace's tidal equations: if the homogeneous equations are used one obtains the normal modes; if the forcing terms are included then the forced solution is obtained. In both cases the solution is obtained numerically. The surface height field is only dependent on the velocity potential orthogonal functions. The expansion coefficients of these functions can be estimated in a least-square sense from available selected tidal measurements.

## 2. BASIC EQUATIONS

### Free Solutions

The method of approach was developed originally by Proudman (1918) using a Lagrangian approach. It was reformulated by Rao (1966) from the Eulerian point of view. The basic ideas of the method presented below follow Rao's line of development. The basic equations are the linearized shallow water equations on a rotating plane:

$$\frac{\partial \vec{M}}{\partial t} - f[\vec{M}] = -g\,\overline{H}h\,\nabla\eta$$

$$\frac{\partial \eta}{\partial t} + \nabla \cdot \vec{M} = 0 \qquad (2.1)$$

where

$$\vec{M} \equiv H\vec{V} \equiv (M,N)$$

$$\vec{V} \equiv (u,v)$$

$$f \equiv 2\omega\sin\theta$$

$$h(x,y) \equiv H(x,y)/\overline{H}.$$

$H(x,y)$ is the variable depth of the fluid in equilibrium and $\overline{H}$ is some constant scaling depth, f is the coriolis parameter, $\vec{V}$ is the horizontal velocity vector, $\eta$ the fluctuation of the free surface. g is the apparent gravitational acceleration and $\nabla$ is the horizontal gradient operator. []: denotes rotation of the vector through a right angle in the clockwise direction of the horizontal plane, i.e. $[] = -(\vec{k} \times \nabla)$, $\vec{k}$ being a unit vector vertical to the horizontal plane.

The appropriate boundary conditions to be adjoined to equations (2.1) are

$$\vec{M} \cdot \vec{n} = 0 \tag{2.2}$$

on the coast, where $\vec{n}$ is the unit normal to the coast line.

The transport vector $\vec{M}$ may be partitioned as follows:

$$\vec{M} = \vec{M}^{\phi} + \vec{M}^{\psi} \tag{2.3}$$

where

$$\vec{M}^{\phi} = -h\,\nabla\phi$$

$$\vec{M}^{\psi} = -[\nabla\psi] \tag{2.4}$$

$\vec{M}^{\psi}$ is the solenoidal part of $\vec{M}$ while $h^{-1}\vec{M}^{\phi}$ is the irrotational part since

$$\nabla\cdot[h^{-1}\vec{M}^{\phi}] = 0$$

$$\nabla\cdot\vec{M}^{\psi} = 0$$

To complete the determination of $\phi$ and $\psi$, it is necessary to specify the boundary conditions $\vec{M}^{\phi} \cdot \vec{n} = 0$ and $M^{\psi} \cdot \vec{n} = 0$ to ensure that eq. (2.2) is satisfied. In terms of $\phi$ and $\psi$ the conditions then are

$$h\frac{\partial\phi}{\partial n} = 0 \tag{2.5}$$

and

$$\psi = 0$$

on the boundaries.

The divergence of the transport field and the vorticity of the velocity field yield

$$\nabla \cdot \vec{M} = -\nabla\cdot h\nabla\phi$$

$$\nabla \cdot [h^{-1}\vec{M}] = \nabla\cdot h^{-1}\nabla\psi \tag{2.6}$$

If $\vec{M}$ is known as a function of the horizontal coordinates, the left-sides of (2.6) are specified. Then each equation represents an inhomogeneous elliptic differential equation with homogeneous boundary conditions given by eq. (2.5), and it is well known that such problems possess a unique solution. It is also straight forward to prove that the representation of $\vec{M}$ as given in eqs. (2.3,4,5) is unique. Since $\vec{M}$ itself is unknown, the procedure then consists of expanding $\phi$ and $\psi$ in terms of the spectra of the elliptic operators appearing in Eq. (2.6); that is, we seek solutions which satisfy the following equations

$$\nabla \cdot h\nabla\phi_\gamma = -\lambda_\gamma\phi$$
$$\nabla \cdot h^{-1}\nabla\psi_\gamma = -\mu_\gamma\psi_\gamma \tag{2.7}$$

where $\phi_\gamma$, $\psi_\gamma$ are the characteristic functions and $\lambda_\gamma$, $\mu_\gamma$ are the characteristic values associated with the corresponding operators $\nabla{\cdot}h\,\nabla$ and $\nabla{\cdot}h^{-1}\nabla$.

The characteristic functions satisfy the boundary conditions

$$h\frac{\partial\phi_\gamma}{\partial n} = 0$$
$$h^{-1}\psi_\gamma = 0 \tag{2.8}$$

The condition $h^{-1}\psi_\gamma = 0$ imposes a stronger condition than that required by (2.5). However, the factor $h^{-1}$ is necessary to make the $\psi_\gamma$ problem self-adjoint. Since the problems (2.7,8) are self-adjoint, the characteristic values $\lambda_\gamma$ and $\mu_\gamma$ are real and the characteristic functions $\phi_\gamma$ and $\psi_\gamma$ each constitute a complete and internally orthogonal set. Without loss of generality, the orthogonality condition may be chosen as:

$$\int h^{-1}\vec{M}_\gamma^\phi\cdot\vec{M}_\beta^\phi dA = \lambda_\gamma\int\phi_\gamma\phi_\beta dA = Ac^2\overline{H}^2\delta_{\gamma\beta},$$
$$\int h^{-1}\vec{M}^\psi{}_\gamma\cdot\vec{M}_\beta^\psi dA = \lambda_\gamma\int\psi_\gamma\psi_\beta dA = Ac^2\overline{H}^2\delta_{\gamma\beta}, \tag{2.9}$$

where $c^2 = gH$ and A is the surface area of the basin. $\delta_{\gamma\beta}$ is the Kronecker delta. We have further defined, in accordance with (2.4),

$$\vec{M}_\gamma^\phi = -h\nabla\phi_\gamma \text{ and } \vec{M}_\gamma^\psi = -[\nabla\psi_\gamma]$$

in the orthogonality condition (2.9).

The components of the transport vector can now be represented by the sums

$$\vec{M}^\phi = \sum_\gamma P_\gamma\vec{M}_\gamma^\phi,$$
$$\vec{M}^\psi = \sum_\gamma Q_\gamma\vec{M}_\gamma^\psi, \tag{2.10}$$

where $P_\gamma$ and $Q_\gamma$ are the expansion coefficients. The orthogonality conditions ensure that equations (2.10) represent the least squares approximations to $\vec{M}^\phi$ and $\vec{M}^\psi$ if and when the sums span the complete spectra of equations (2.7). The height field $\eta$ is governed by the divergent part of $\vec{M}$ and the $\phi_\gamma$ functions yield a sufficient basis for its representation. A convenient representation for $\eta$ may be taken as:

$$\eta = \sum_\gamma R_\gamma\eta_\gamma,$$
$$\eta_\gamma = c^{-1}(\lambda_\gamma)^{1/2}\phi_\gamma, \tag{2.11}$$

where $R_\gamma$ are the expansion coefficients for the $\eta$-field.

Substitution of equations (2.10) and (2.11) into equations (2.1) and the use of the orthogonality conditions (2.9) yield a set of prediction equations for the expansion coefficients:

$$\frac{dP_\gamma}{dt} - \sum_\beta A_{\gamma\beta}P_\beta - \sum_\beta B_{\gamma\beta}Q_\beta - \vartheta_\gamma R_\gamma = 0$$
$$\frac{dQ_\gamma}{dt} - \sum_\beta C_{\gamma\beta}P_\beta - \sum_\beta D_{\gamma\beta}Q_\beta = 0 \tag{2.12}$$
$$\frac{dR_\gamma}{dt} + \vartheta_\gamma P_\gamma = 0$$

where the coupling coefficients are given by

$$A_{\gamma\beta} \equiv \{\vec{M}^{\beta}_{\gamma}, [\vec{M}^{\phi}{}_{\beta}]\}\ , \qquad B_{\gamma\beta} \equiv \{\vec{M}^{\phi}{}_{\gamma}, [\vec{M}^{\phi}{}_{\beta}]\}\ ,$$
$$C_{\gamma\beta} \equiv \{\vec{M}^{\psi}_{\gamma}, [\vec{M}^{\phi}{}_{\beta}]\}\ , \qquad D_{\gamma\beta} \equiv \{\vec{M}^{\psi}{}_{\gamma}, [\vec{M}^{\psi}{}_{\beta}]\}\ , \tag{2.13}$$

The quantity inside the angular brackets represents an inner product of two vectors $\vec{W}$ and $\vec{T}$ and is denoted by

$$\{\vec{W},\vec{T}\} = (1/c^2\ A\overline{H}^2) \int_A fh^{-1}\ \vec{W}\cdot\vec{T}dA.$$

It can be seen from eq. (2.12, 13) and the definition of the inner product that all the coupling coefficients vanish when the coriolis parameter $f=0$ and hence

$$\frac{d^2P_\gamma}{dt^2} + \vartheta^2{}_\gamma P_\gamma = 0.$$

$\vartheta_\gamma = (c^2\lambda_\gamma)^{1/2}$, is the non-rotating frequency of oscillation.

In equations (2.12, 13) the subscript $\gamma$ (or $\beta$) is used as a proxy for a binary index and represents an ordering of the characteristic functions $\phi_\gamma$, $\psi_\gamma$ in some as yet unspecified manner. For convenience we replace the wavenumber index $\gamma$ by scalar indices $i=1,2,3$ (or $j=1,2,3\ldots$) and denote

$$\begin{gathered}
\lambda_i \equiv \lambda_{\gamma i},\ M_i \equiv M_{\gamma i},\ \vartheta_i \equiv \vartheta_{\gamma i} \\
P_i \equiv P_{\gamma i},\ \equiv Q_{\gamma i},\ R_i \equiv R_{\gamma i} \\
A_{ij} \equiv A_{\gamma i\beta j} \\
B_{ij} \equiv B_{\gamma i\beta j} \\
C_{ij} \equiv C_{\gamma i\beta j} \\
D_{ij} \equiv D_{\gamma i\beta j}
\end{gathered} \tag{2.14}$$

Using the above notation, we can define column vectors

$$\vec{P} \equiv \text{col}\ (P_i),\ \vec{Q} = \text{col}\ (Q_i),\ \vec{R} = \text{col}\ (R_i)$$

$$S \equiv \begin{vmatrix} \vec{P} \\ \vec{Q} \\ \vec{R} \end{vmatrix} \tag{2.15a}$$

and matrices

$$\begin{gathered}
\underset{\sim}{A} \equiv \{\ A_{ij}\ \},\ \underset{\sim}{B} \equiv \{\ B_{ij}\ \} \\
\underset{\sim}{C} \equiv \{\ C_{ij}\ \},\ \underset{\sim}{D} \equiv \{\ D_{ij}\ \} \\
<\vartheta> \equiv \text{diagonal}\ \vartheta_i
\end{gathered} \tag{2.15b}$$

Equations (2.12) may now be written in the form

$$\frac{d\vec{s}}{dt} + \underset{\sim}{a}\ \vec{s} = 0 \tag{2.16}$$

where $\underset{\sim}{a}$ is the square matrix

$$\underset{\sim}{a} \equiv \begin{vmatrix} -A & -B & -\langle\vartheta\rangle \\ -C & -D & 0 \\ \langle\vartheta\rangle & 0 & 0 \end{vmatrix} \tag{2.17}$$

In seeking the solutions for the normal modes, we assume

$$\vec{s} \sim e^{i\sigma t}$$

where $\sigma$ is the normal mode frequency with rotation and $i \equiv \sqrt{-1}$. Eq. (2.15) then reduces to

$$(\sigma II - i\underset{\sim}{a})\,\vec{s} = 0. \tag{2.18}$$

In the preceding equation II is the identity matrix. $\sigma$'s are the characteristic values of the matrix $i\underset{\sim}{a}$. From the definition of the coupling coefficients given in (2.13) and the matrix $\underset{\sim}{a}$ as defined in (2.17), it is clear that $i\underset{\sim}{a}$ exhibits Hermitian symmetry and hence the $\sigma$'s constitute a spectrum of real eigenvalues. In computing the matrix elements in $\underset{\sim}{a}$, the basis functions $\phi_i$ and $\psi_i$ are chosen to correspond to an ordering of the characteristic values $\lambda_i$ and $\mu_i$ arranged so that $\lambda_1 < \lambda_2 < \lambda_3 \ldots$ and $\mu_1 < \mu_2 < \mu_3 \ldots$ . Such an ordering has been chosen since the $\lambda_i$'s and $\mu_i$'s have the dimensions of (wavenumber)$^2$. Hence, at any order of truncation, those $\phi_i$'s and $\psi_i$'s with the largest space scales are taken into account.

**Forced Solution**

In the computation of the forced solution we include the effects of the yielding of the solid earth to tide generating forces. The effects due to self-attraction of the tide and tidal loading as well as the frictional effects have not been included. The theory allows for the inclusion of these effects but they introduce computational complications and physical uncertainties and they are not necessary in the context of the application of the interpolation technique. Equations (2.1) are recast for the forced tidal oscillations as

$$\begin{aligned} \frac{\partial \vec{M}}{\partial t} - f[\vec{M}] &= -g\overline{H}h\nabla\eta', \\ \frac{\partial \eta}{\partial t} + \nabla.\vec{M} &= 0, \end{aligned} \tag{2.19}$$

where

$$\eta' = \eta - (1 + k_2 - h_2)\bar{\eta}.$$

$k_2, h_2$ are the Love numbers and $\bar{\eta}$ is the equilibrium tide height. Let the vector $\vec{G} = g\overline{H}h\,(1+k_2-h_2)\nabla\bar{\eta}$. Equations (2.19) can then be written

$$\begin{aligned} \frac{\partial \vec{M}}{\partial t} - f[\vec{M}] &= -g\overline{H}h\nabla\eta + \vec{G} \\ \frac{\partial \eta}{\partial t} + \nabla.\vec{M} &= 0, \end{aligned} \tag{2.20}$$

Substitution of the expansions (2.10) and (2.11) into equations (2.20) yields, after using (2.13)

$$\begin{aligned} \frac{dP_\gamma}{dt} - \sum_\beta A_{\gamma\beta}P_\beta - \sum_\beta B_{\gamma\beta}Q_\beta - \vartheta_\gamma R_\gamma &= (c^2A\overline{H}^2)\int fh^{-1}\vec{G}\cdot\vec{M}_\gamma^\phi dA \\ \frac{dQ_\gamma}{dt} - \sum_\beta C_{\gamma\beta}P_\beta - \sum_\beta D_{\gamma\beta}Q_\beta &= (c^2A\overline{H}^2)^{-1}\int fh^{-1}\vec{G}\cdot\vec{M}_\gamma^\psi dA \\ \frac{dR_\gamma}{dt} + \vartheta_\gamma P_\gamma &= 0 \end{aligned} \tag{2.21}$$

Define the vector $\vec{F}$ as follows,

$$\vec{F} = \begin{vmatrix} (c^2 A\overline{H}^2)^{-1} \int f h^{-1} \vec{G} \cdot \vec{M}_\gamma^\phi dA \\ (c^2 A\overline{H}^2)^{-1} \int f h^{-1} \vec{G} \cdot \vec{M}_\gamma^\phi dA \\ 0 \end{vmatrix} \tag{2.22}$$

Equations (2.21) can then be written as an inhomogeneous matrix equation

$$\frac{d\vec{S}}{dt} + \underset{\sim}{a}\vec{S} = \vec{F}, \tag{2.23}$$

where $\vec{S}$ and $\underset{\sim}{a}$ are defined by equations (2.15a) and (2.17). The solution of equation (2.23) is given by

$$\vec{S} = \underset{\sim}{C} \langle e^{i\sigma t} \rangle \int_o^t \langle e^{-i\sigma\tau} \rangle \underset{\sim}{C}^{-1} \vec{F}(\tau)\, d\tau, \tag{2.24}$$

where

$\underset{\sim}{C}$ is the modal matrix containing the eigenvectors of $\underset{\sim}{a}$ arranged in columns and $\sigma$ are the characteristics values of $\underset{\sim}{a}$. $\langle e^{i\sigma t} \rangle$ is a diagonal matrix.

## 3. OBJECTIVE ANALYSIS

**The orthogonal functions** $\phi_\gamma$ form a basis for the expansion of the height field $\eta$, as discussed earlier. Since these functions are characteristic for a particular basin and are described at all points inside the basin (within the resolution of the finite difference grid), they can be used as optimal functions for extrapolation of the tidal field over the whole basin, given data at some selected points.

Even through the basis functions are orthogonal, in fitting the data to these functions it is preferable to use linear least-squares techniques to determine the coefficients of expansion rather than the orthogonality property since real data are not usually available at regularly spaced points. A similar approach was taken in a previous investigation by Rao and Schwab (1981) in which they determined the steady circulation in a closed basin for which the appropriate orthogonal functions are the $\psi_\gamma$ functions and Sanchez et al. (1985) used the $\phi_\gamma$ functions for tidal extrapolation in Lake Superior. An outline of the procedure and the basic equations involved are given below.

The tidal height field as given by equations (2.11) and (2.15) can be written

$$\eta(x,y,t) = \sum_\gamma R_{\gamma r}\, \eta_\gamma(x,y) \cos\sigma t - \sum_\gamma R_{\gamma I}\, \eta_\gamma(x,y) \sin\sigma t \tag{3.1}$$

where $R_{\gamma r}$ and $R_{\gamma I}$ denote the real and imaginary parts of $R_\gamma$. The tidal height field can be expressed also in terms of amplitude $A(x,y)$ and phase $\Theta(x,y)$, that is

$$\eta(x,y,t) = A(x,y) \cos\,[\sigma t - \Theta(x,y)] \tag{3.2}$$

Comparing equations (3.1) and (3.2) one obtains the following relations,

$$\begin{aligned} A(x,y) &= [(\sum_\gamma R_{\gamma r}\, \eta_\gamma)^2 + (\sum_\gamma R_{\gamma I}\, \eta_\gamma)^2]^{1/2} \\ \Theta(x,y) &= \arctan\,[-(\sum_\gamma R_{\gamma I}\, \eta_\gamma)/(\sum_\gamma R_{\gamma r}\, \eta_\gamma)] \end{aligned} \tag{3.3}$$

Also, from equations (3.1) and (3.2) one obtains the following vector-matrix relations

$$\begin{aligned} [\underset{\sim}{\eta}]\, \vec{R}_r &= \vec{A} \cos\Theta \\ [\underset{\sim}{\eta}]\, \vec{R}_I &= \vec{A} \sin\Theta \end{aligned} \tag{3.4}$$

The components of the vectors $\vec{A}\cos\Theta$ and $\vec{A}\sin\Theta$ are the "n" available tidal measurements. The matrix $[\underset{\sim}{\eta}]$ is available from the solution of the velocity potential eigenfunctions, its "k" columns will correspond to the velocity potential eigenfunctions chosen to represent the forced solution, its "n" rows correspond to the location of the tidal measurements in the basin under consideration. The least squares solution to equations (3.4) is then given by

$$\begin{aligned} \vec{R}_r &= ([\underset{\sim}{\eta}]^T[\underset{\sim}{\eta}])^{-1}[\underset{\sim}{\eta}]^T \vec{A}\ \cos\Theta, \\ \vec{R}_I &= ([\underset{\sim}{\eta}]^T[\underset{\sim}{\eta}])^{-1}[\underset{\sim}{\eta}]^T \vec{A}\ \sin\Theta, \end{aligned} \tag{3.5}$$

where $[\underset{\sim}{\eta}]^T$ is the transposed matrix. Having determined a certain number of coefficients $\vec{R}_r$ and $\vec{R}_I$, since the functions $\eta_\gamma(x,y)$ are known over the entire basin, one can obtain the amplitude and phase of the tidal height at all points in the basin from eq. (3.3). The maximum number of coefficients $\vec{R}_r$ and $\vec{R}_I$ that can be determined will be the same as the number of observations available.

## 4. RESULTS

### Normal Modes and Forced Solutions

A normal mode solution for the Atlantic and Indian oceans has been obtained by means of a 6° × 6° finite difference grid. There are 462 velocity potential and 370 stream function points distributed such as to form a single Richardson lattice. A finite difference solution of equations (2.7) subject to the boundary conditions given by equations (2.8) yields the eigenvalues and eigenvectors for both fields. The eigenfunctions of the Θ solution represent the non-rotating gravitational normal modes of the basin, the periods of oscillation of the lowest modes are given in the second column of Table 1. The stream

**TABLE 1. GRAVITATIONAL MODES**

| PERIOD (HOURS) | | ENERGY RATIO |
|---|---|---|
| ROTATIONAL | NON-ROTATIONAL | (KINETIC/POTENTIAL) |
| 67.92 | 77.68 | 1.47 |
| 42.53 | 40.98 | 0.96 |
| 29.61 | 29.00 | 0.81 |
| 23.55 | 22.17 | 0.84 |
| 20.93 | 20.73 | 0.86 |
| 19.40 | 19.20 | 1.19 |
| 17.34 | 19.08 | 1.03 |
| 15.73 | 16.52 | 1.11 |
| 14.44 | 14.56 | 0.86 |
| 13.93 | 14.17 | 1.03 |
| 12.99 | 13.42 | 1.07 |
| 12.55 | 12.94 | 1.27 |
| 11.99 | 12.74 | 1.09 |
| 11.13 | 11.72 | 1.14 |
| 10.93 | 11.47 | 1.14 |
| 10.62 | 11.12 | 1.15 |
| 10.39 | 10.60 | 1.21 |
| 9.97 | 10.26 | 1.16 |
| 9.52 | 9.99 | 1.19 |
| 9.21 | 9.26 | 1.00 |

function modes generate the vorticity component of the flow field in the rotating case for the gravitational and rotational species, they are more dominant for the quasi-geostrophic rotational modes than for the gravitational modes. The normal mode solution was obtained by including the lowest 150 eigenfunctions from each field ($\phi$ and $\psi$ ) into the dynamical equations, the solution of the eigenvalue problem posed by equation (2.18) yields the normal modes. The normal modes fall into two distinct categories: the inertia-gravitational modified by rotation and the rotational modified by divergence. If the secular determinant is truncated at a size n x n, then one obtains 2n/3 gravitational modes and n/3 rotational modes, in pairs (plus and minus the same value). In our case there are 300 gravitational modes and 150 rotational modes. The rotational modes are characterized by high ratios of kinetic to potential energy, these modes will vanish in a basin of constant depth and Coriolis parameter. The rotational normal modes are extremely sensitive to the resolution of the shape of the basin and the bottom topography and the convergence of their roots is more complicated than for gravitational modes. A detailed discussion of the nature of the two types of modes is given by Platzman (1975) and Rao and Schwab (1976). The gravitational modes are by far the most important in the context of the diurnal and semidiurnal tides as shown by Platzman (1984).

Table 1 gives a list of the first 20 gravitational modes in order of decreasing period, for each mode the following quantities are given: the rotational and non-rotational periods in hours, the ratio of energies (kinetic/potential).

Table 2 lists the 20 most powerful modes for the M2 and K1 tidal components in order of decreasing power. The entries in the table give the power ranking, the rotational period in hours, the percentage of the total power for that mode and the percentage of the total power contributed by all the modes included up to that point.

**TABLE 2. POWER SPECTRUM FOR THE M2 AND K1 COMPONENTS**

| | M2 | | | K1 | | |
|---|---|---|---|---|---|---|
| RANK | PERIOD (HOURS) | POWER (%) EACH | SUM | PERIOD (HOURS) | POWER (%) EACH | SUM |
| 1 | 12.99 | 7.67 | 7.67 | 23.55 | 12.79 | 12.79 |
| 2 | 10.62 | 7.33 | 15.01 | 13.93 | 8.70 | 21.49 |
| 3 | 13.93 | 7.31 | 22.32 | 17.34 | 8.19 | 29.68 |
| 4 | 11.99 | 6.00 | 28.33 | 20.93 | 8.01 | 37.70 |
| 5 | 14.44 | 5.34 | 33.67 | 29.61 | 3.52 | 41.23 |
| 6 | 10.39 | 3.84 | 37.51 | 15.73 | 3.47 | 44.70 |
| 7 | 12.55 | 3.61 | 41.13 | 19.40 | 3.37 | 48.08 |
| 8 | 9.21 | 3.44 | 44.58 | 12.99 | 2.92 | 51.00 |
| 9 | 19.40 | 2.95 | 47.53 | 10.93 | 2.82 | 53.82 |
| 10 | 17.34 | 2.74 | 50.28 | 11.13 | 2.62 | 56.45 |
| 11 | 9.52 | 2.68 | 52.96 | 9.21 | 2.15 | 58.60 |
| 12 | 8.92 | 2.62 | 55.59 | 67.92 | 2.04 | 60.65 |
| 13 | 11.13 | 2.52 | 58.12 | 14.44 | 1.62 | 62.28 |
| 14 | 8.30 | 2.41 | 60.53 | 8.80 | 1.61 | 63.90 |
| 15 | 9.97 | 1.62 | 62.16 | 8.30 | 1.58 | 65.49 |
| 16 | 8.01 | 1.55 | 63.71 | 11.99 | 1.46 | 66.95 |
| 17 | 23.55 | 1.54 | 65.25 | 9.97 | 1.36 | 68.31 |
| 18 | 8.70 | 1.44 | 66.70 | 12.55 | 1.34 | 69.66 |
| 19 | 8.09 | 1.43 | 68.14 | 10.39 | 1.34 | 71.00 |
| 20 | 7.82 | 1.40 | 69.54 | 8.40 | 1.14 | 72.15 |

The three most powerful modes in the M2 spectrum are the modes with periods of 12.99 hours (7.67%), 10.62 hours (7.33%) and 13.93 hours (7.31%). For the K1 spectrum the three most powerful modes have periods of 23.55 hours (12.79%), 13.93 hours (8.70%) and 17.34 hours (8.19%). Figures 1 to 5 below give the structure (amplitude and phase) for these 5 modes. The amplitudes have been normalized to a maximum value of 100, the amplitude contours are shown by the solid lines and the dotted lines correspond to the phases.

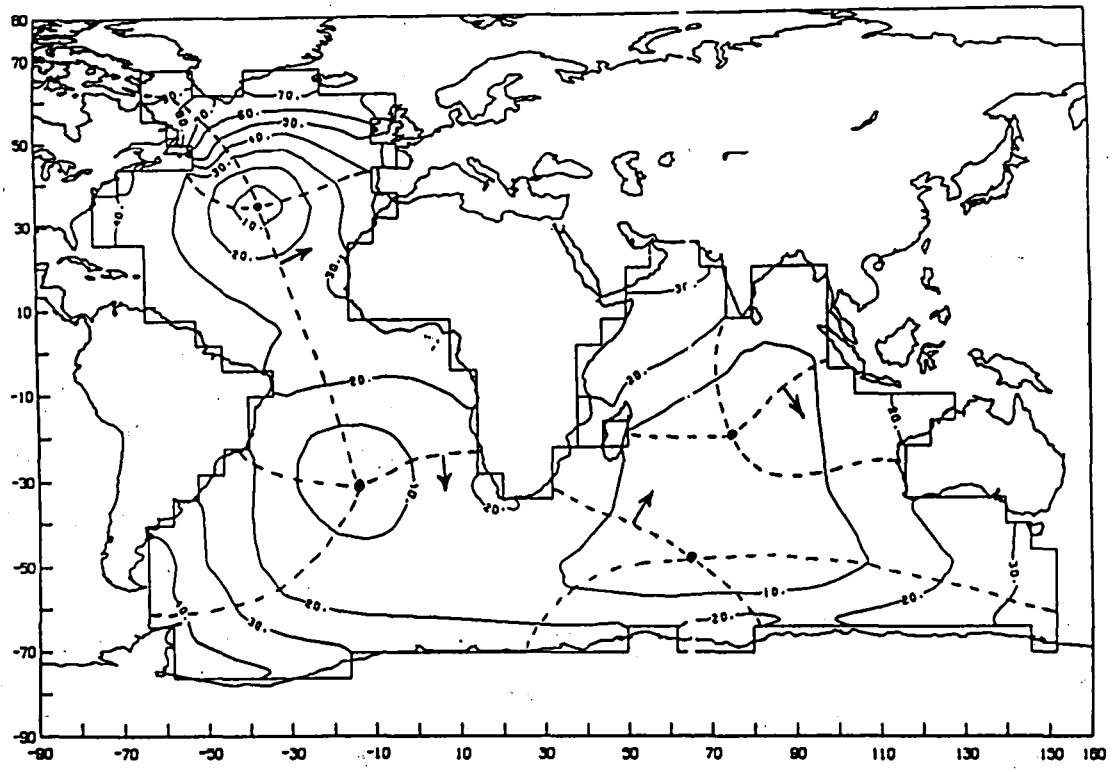

Figure 1. Normal Mode, Period = 23.55 Hours

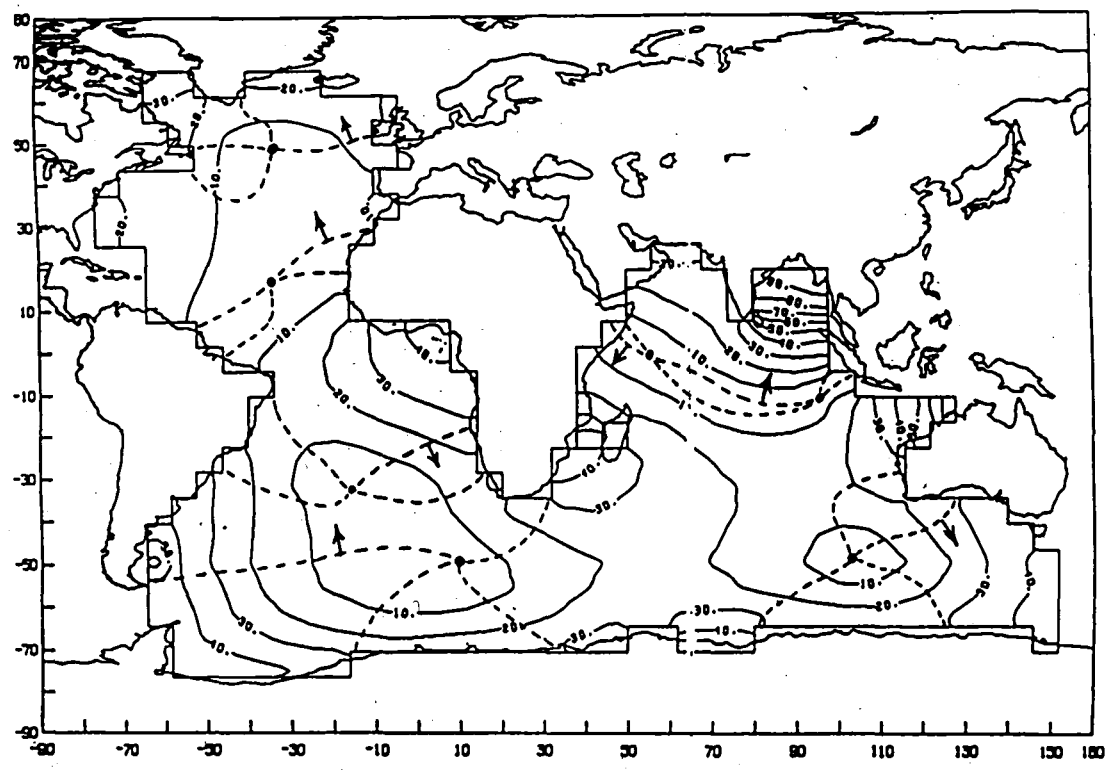

Figure 2. Normal Mode, Period = 17.34 Hours

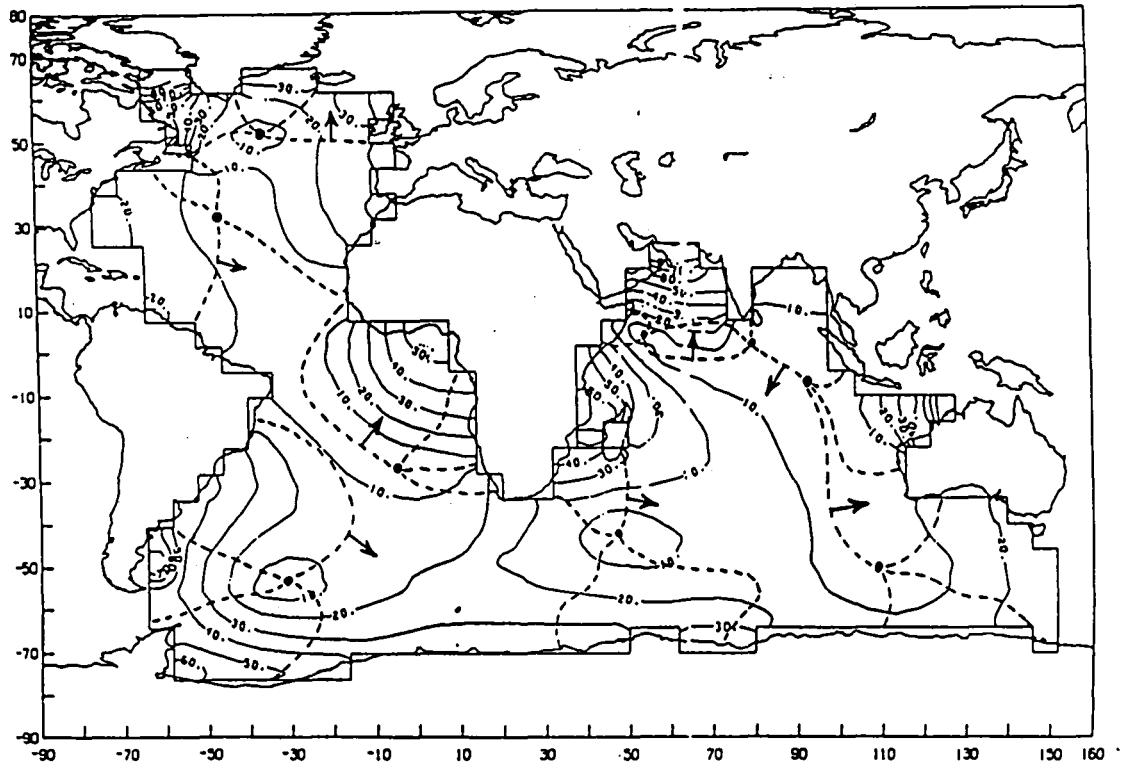


**Figure 3. Normal Mode, Period = 13.93 Hours**

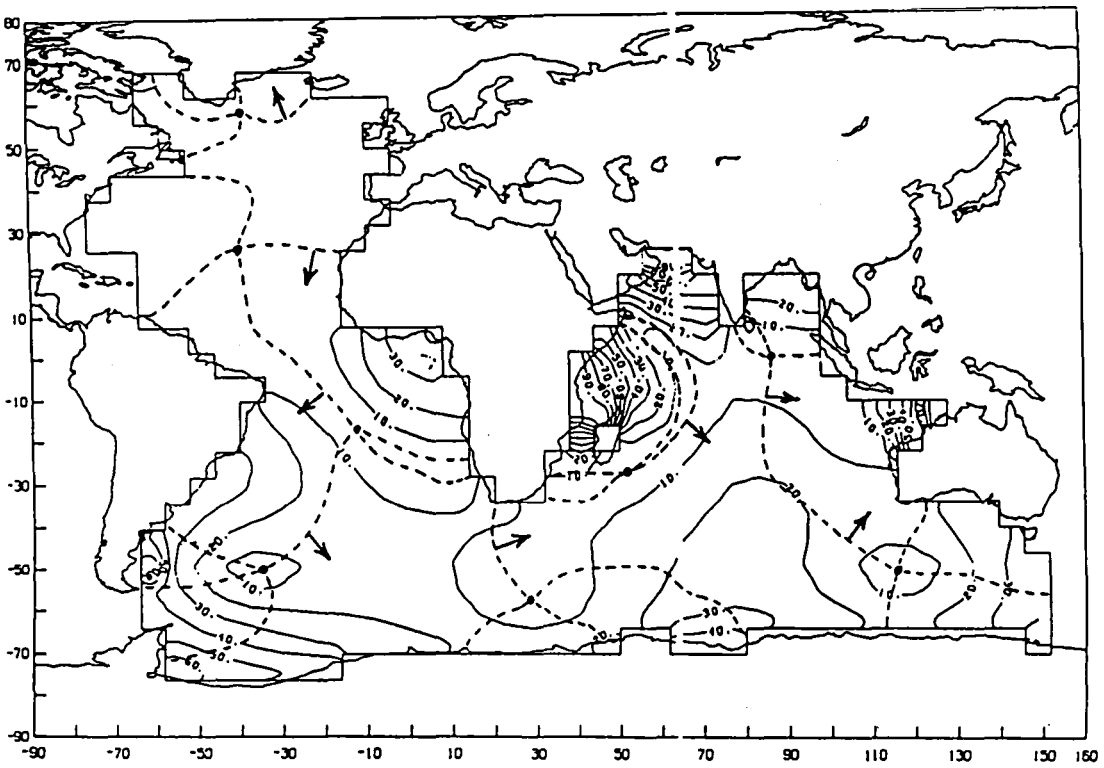


**Figure 4. Normal Mode, Period = 12.99 Hours**

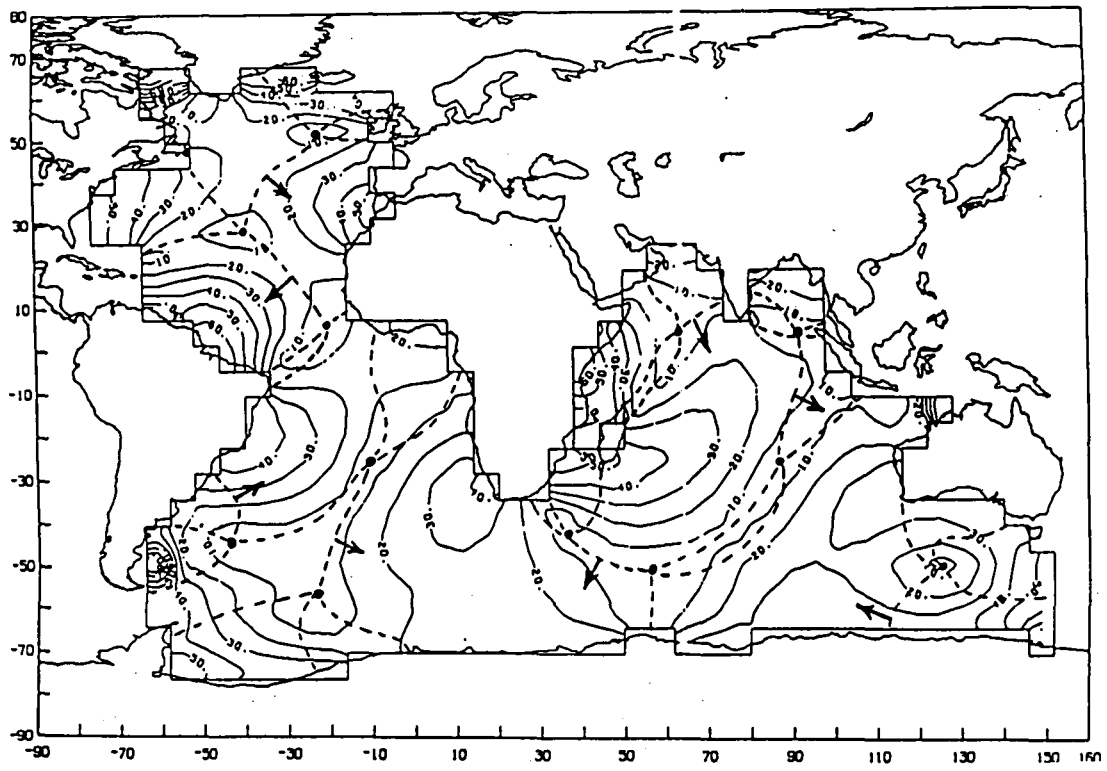


**Figure 5. Normal Mode, Period = 10.62 Hours**

Figures 6 and 7 show the M2 and K1 tidal solutions. These solutions were obtained by including the first 150 eigenfunctions from the $\phi$ and $\psi$ solutions. The forced solution for $\eta$ then contains 150 coefficients $R_\gamma$. The contours of equal amplitude and phase are given by the solid and dotted lines respectively. The arrows indicate the sense of progression for high and low water.

The solution for the M2 tide shows an amphidromic point south of Greenland and a double amphidromic system in the central North Atlantic. There is an amphidrome in the South Atlantic and several amphidromes in the periphery of the Indian Ocean, the central Indian Ocean shows the usual anti-amphidromic high. The K1 tide shows a simpler structure with amphidromic points in the central North and South Atlantic and two amphidromes in the Indian Ocean. The M2 solution has an amplitude rms of 51.6 cm, the corresponding value for K1 is 26 cm.

Figures 8 and 9 show the approximate location of the amphidromes for the M2 and K1 tidal solutions as obtained by different investigators. The different models agree fairly well with each other in certain areas and show wide variations in other regions. The results of our model are reasonable, undoubtedly much of the variations can be attributed to poor resolution due to the coarseness of the 6° × 6° grid as well as the absence of frictional effects, self-attraction and tidal loading.

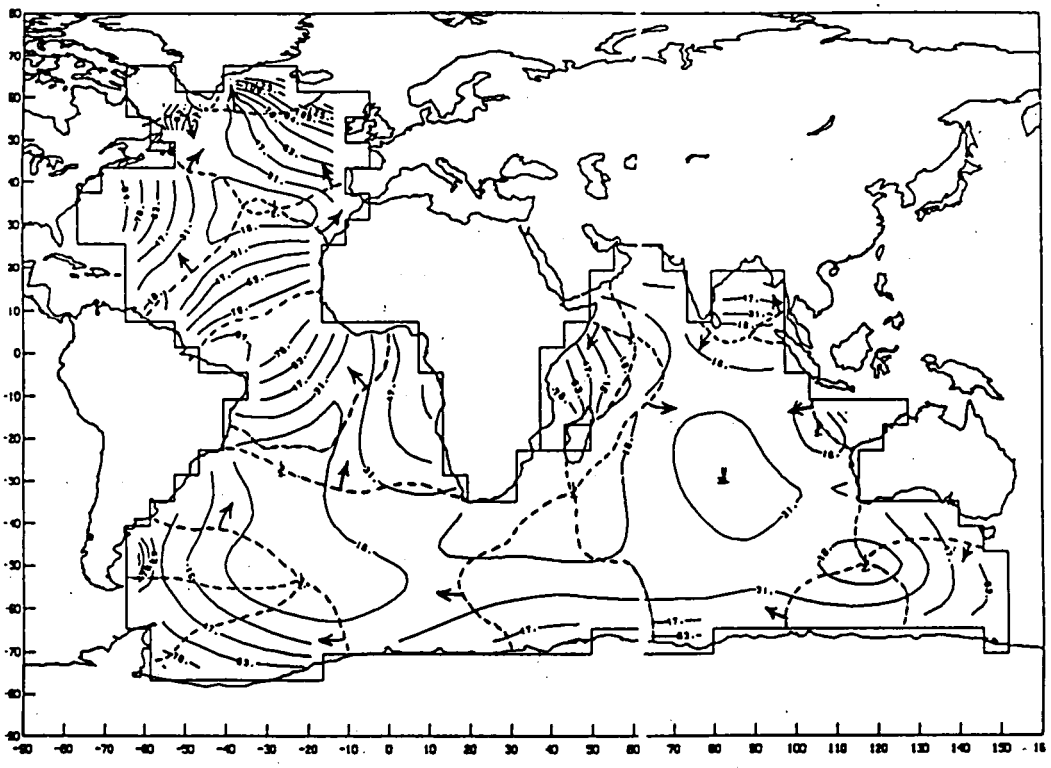

Figure 6. M2 Tidal Solution

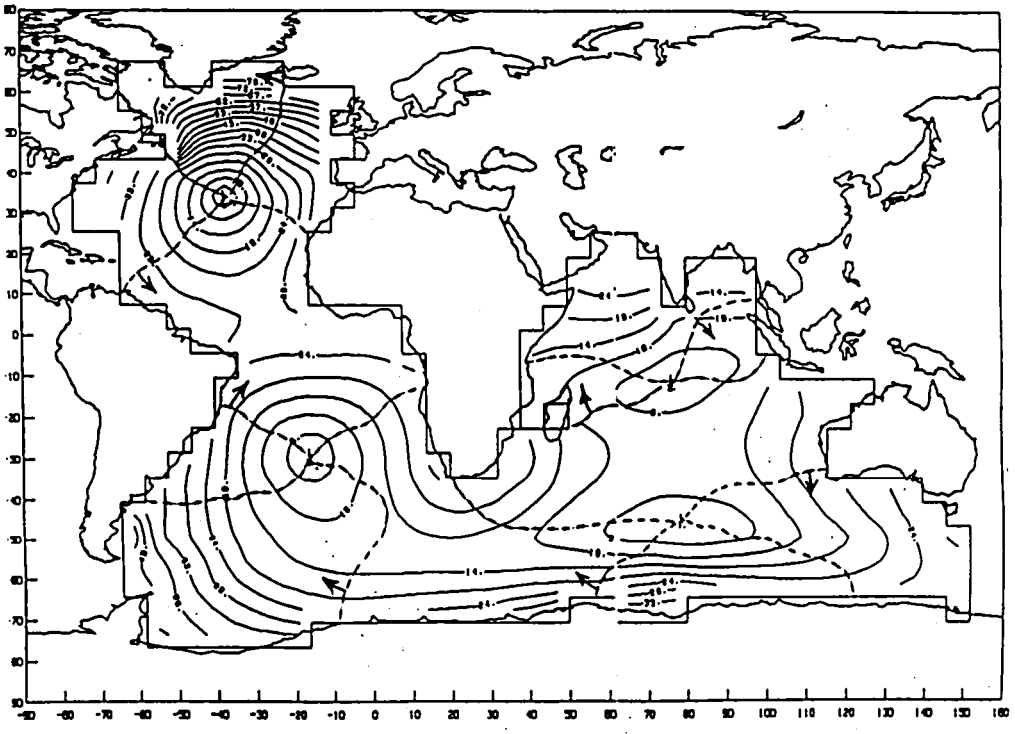

Figure 7. K1 Tidal Solution

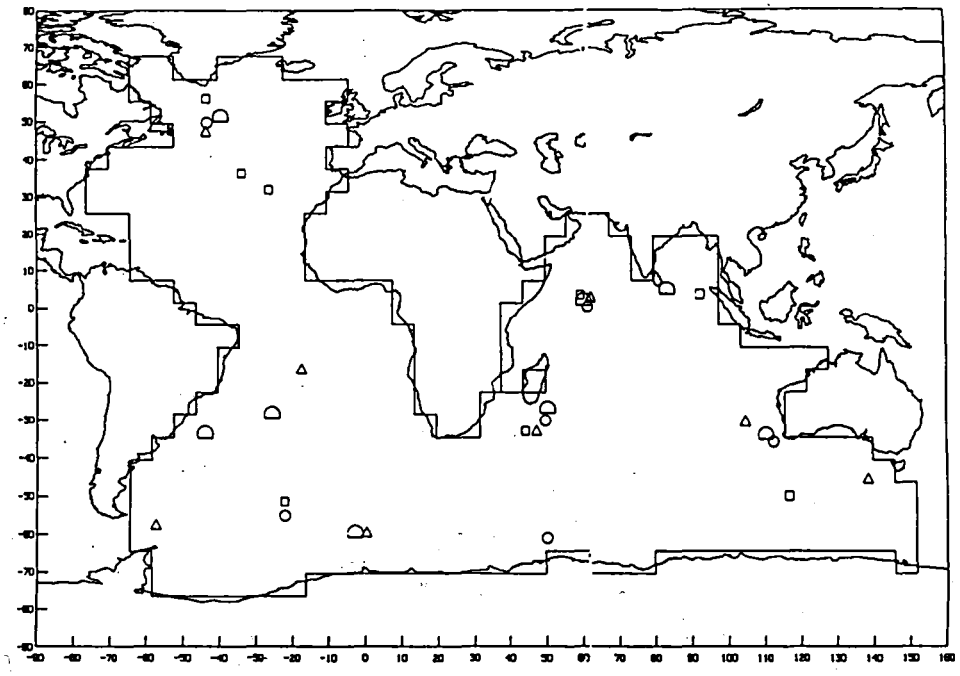

**Figure 8. Location of Amphidromes for the M2 Tide**

○: Schwiderski (1979)
○: Parke and Hendershott (1980)
△: Accad and Pekeris (1978)
□: This Investigation

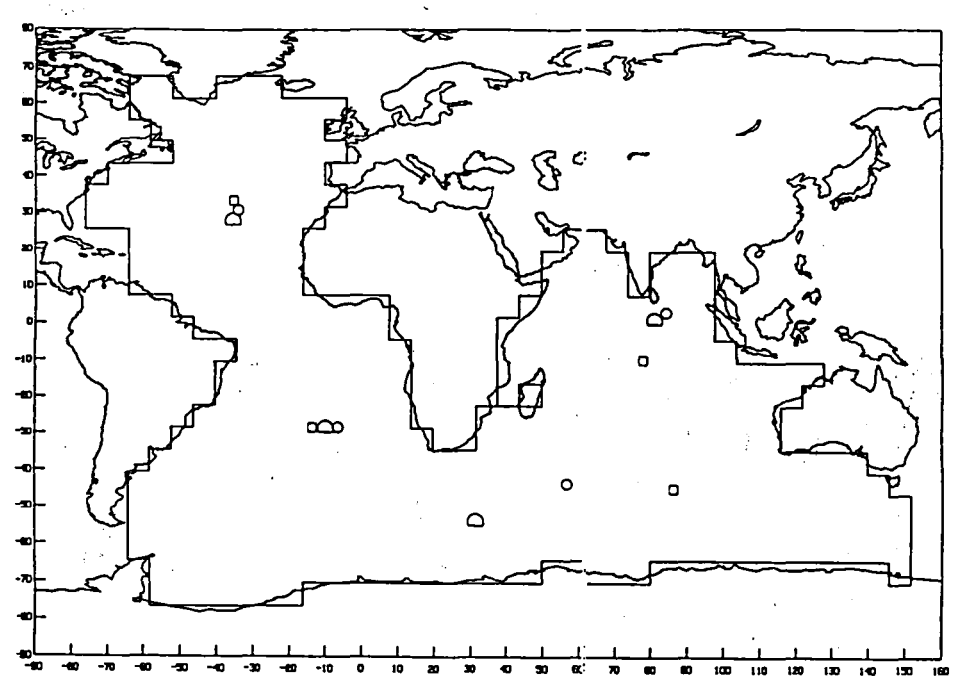

**Figure 9. Location of Amphidromes for the K1 Tide**

○: Schwiderski (1981)
○: Parke and Hendershott (1980)
□: This Investigation

## Objective Analysis Evaluation

In the objective analysis of the tide we attempt to use the data wherever they are available and fit co-range and co-tidal lines to describe the tide over the entire basin using the velocity potential eigenfunctions in a least squares sense. Since the actual tidal distribution over the entire basin is unknown, it is not possible to answer the question of how well this extrapolation procedure has worked. We have chosen to use the theoretically simulated tidal field as the "true solution" and compare the resulting tidal pattern obtained from a selected set of data points. The theoretical simulation also serves as a guide in choosing the most energetic modes to be used in the objective analysis. Ideally, in the least squares procedure it is preferable to use fewer functions than there are available data points to ensure a smooth fit and employ an *a priori* knowledge of the most dominant modes in making this selection.

In order to carry out the testing of the objective analysis two sets of data points have been created. In one case every fourth point in the $\phi$ field was defined as a data point, yielding the 116 data points shown in Figure 10. In the second case every sixth point was taken, to obtain the 77 data points shown in Figure 11. The tidal amplitudes and phases at these points were extracted from the theoretical simulation of the M2 tide using 150 modes.

A comparison of the objectively analyzed amplitudes and phases with the "true" values at all grid points is shown in Tables 3 and 4. The tables list the percentage of total grid points (462) where the analyzed and true values of amplitude and phase agree with each other within the limits indicated for the different cases corresponding to the number of modes chosen in the analysis. Also given in the table are the rms errors of the amplitude over the entire basin and only at the data points.

In addition the two data sets were objectively analyzed using spherical harmonics. The results are shown in Tables 5 and 6. These tables list the same quantities as in Tables 3 and 4 for the different cases corresponding to the degree of the expansion chosen for the fit.

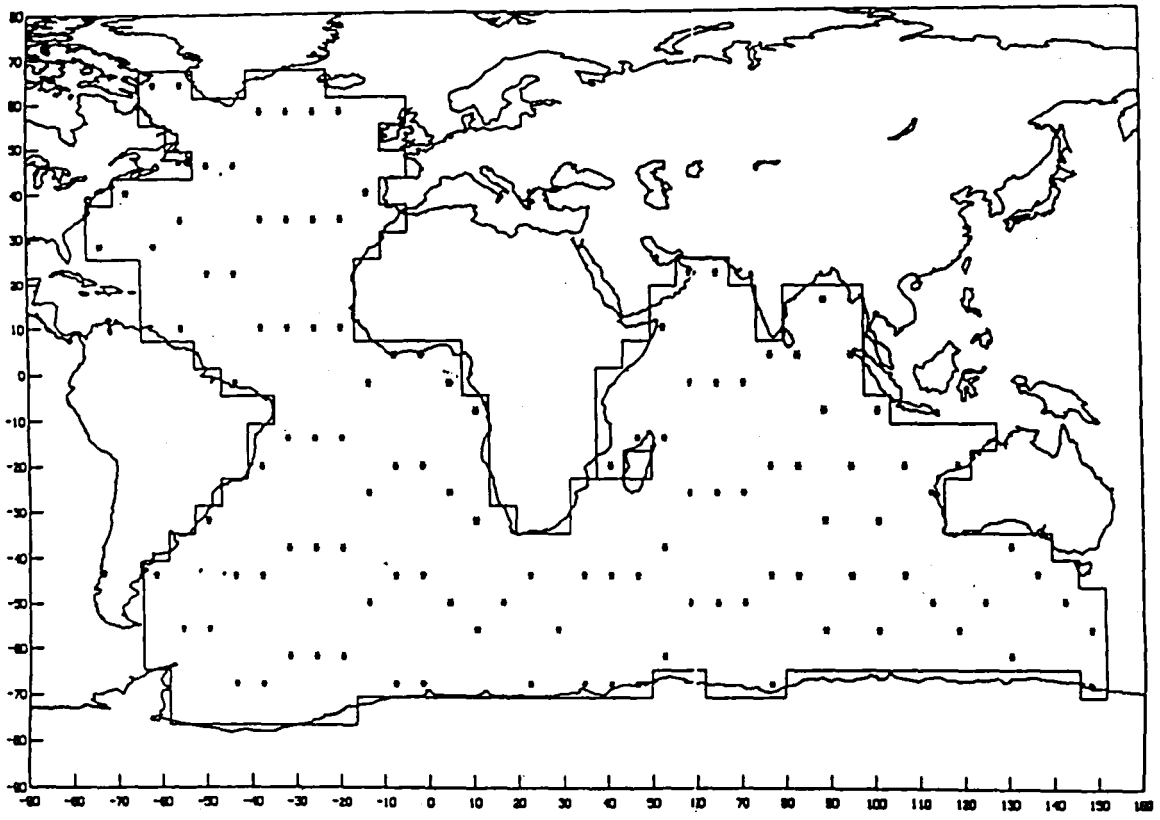

**Figure 10. Data Set (116 Points)**

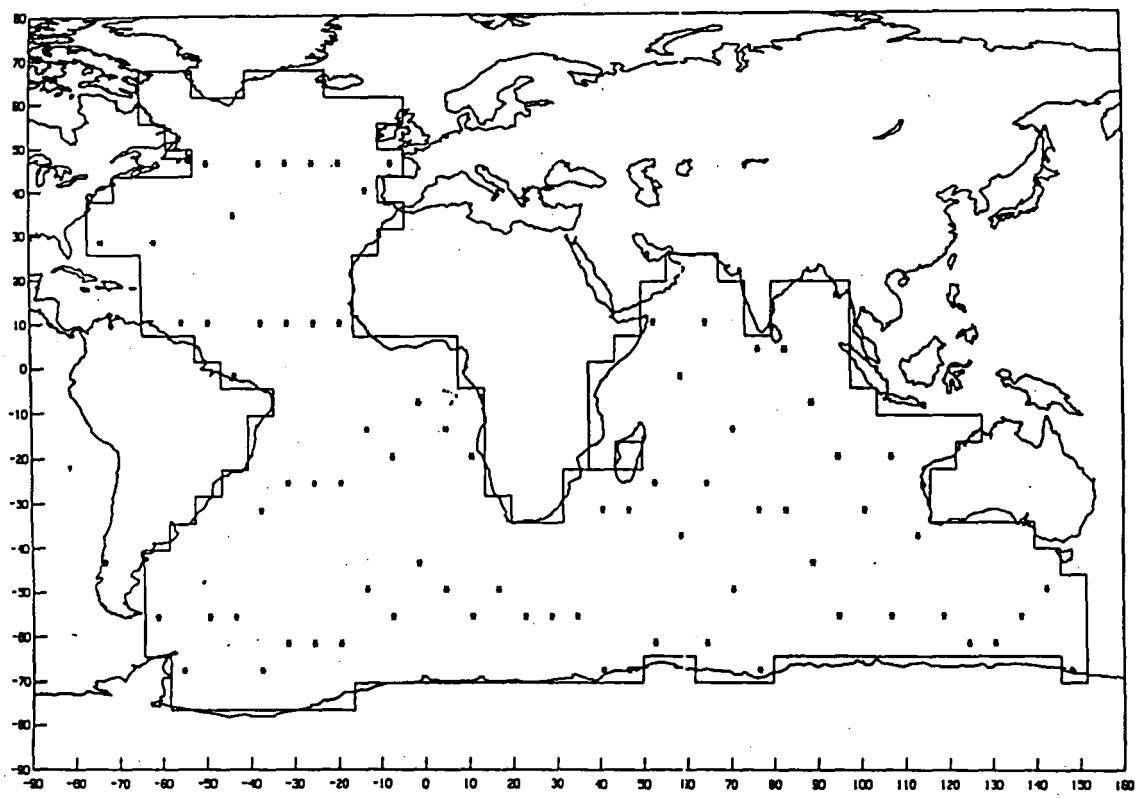

**Figure 11. Data Set (77 Points)**

**TABLE 3. COMPARISON BETWEEN OBJECTIVELY ANALYZED AND THEORETICAL FIELDS .M2 COMPONENT. (116 data points)**

| Coefficients (% of Total Power) | | Amplitude (%) | | | Phase (%) | | | RMS (cm) | |
|---|---|---|---|---|---|---|---|---|---|
| | | <5% | <10% | <20% | <5° | <10° | <20° | TOTAL | DATA |
| 14 | (60.5) | 14 | 27 | 48 | 29 | 48 | 71 | 11.6 | 9.4 |
| 29 | (78.5) | 35 | 55 | 79 | 51 | 75 | 90 | 5.4 | 3.6 |
| 39 | (84.4) | 37 | 60 | 83 | 56 | 78 | 94 | 7.1 | 2.7 |
| 48 | (88.0) | 47 | 69 | 88 | 65 | 84 | 95 | 7.0 | 2.0 |
| 58 | (90.8) | 53 | 78 | 92 | 68 | 87 | 97 | 4.2 | 1.6 |
| 68 | (92.8) | 56 | 74 | 89 | 73 | 84 | 92 | 9.1 | 0.9 |
| 80 | (94.7) | 58 | 73 | 88 | 76 | 89 | 96 | 19.5 | 0.6 |

**TABLE 4. COMPARISON BETWEEN OBJECTIVELY ANALYZED AND THEORETICAL FIELDS .M2 COMPONENT. (77 data points)**

| Coefficients (% of Total Power) | | Amplitude (%) <5% | <10% | <20% | Phase (%) <5° | <10° | <20° | RMS (cm) TOTAL | DATA |
|---|---|---|---|---|---|---|---|---|---|
| 8 | (44.5) | 8 | 18 | 31 | 9 | 18 | 37 | 18.8 | 17.2 |
| 14 | (60.5) | 14 | 27 | 51 | 30 | 50 | 70 | 13.6 | 9.8 |
| 19 | (68.1) | 16 | 34 | 58 | 35 | 55 | 79 | 12.4 | 7.8 |
| 24 | (74.0) | 26 | 43 | 68 | 36 | 60 | 83 | 12.9 | 4.7 |
| 29 | (78.5) | 35 | 55 | 78 | 44 | 63 | 86 | 10.4 | 2.9 |
| 32 | (80.4) | 32 | 57 | 78 | 43 | 63 | 86 | 8.6 | 2.5 |
| 34 | (81.6) | 34 | 55 | 78 | 46 | 68 | 88 | 15.5 | 1.9 |
| 39 | (84.4) | 32 | 52 | 76 | 46 | 67 | 86 | 35.5 | 1.7 |

**TABLE 5. OBJECTIVE ANALYSIS USING SPHERICAL HARMONICS .M2 COMPONENT. (116 data points)**

| Degree (No. of Coeff.) | | Amplitude (%) <5% | <10% | <20% | Phase (%) <5° | <10° | <20° | RMS (cm) TOTAL | DATA |
|---|---|---|---|---|---|---|---|---|---|
| 2 | (18) | 5 | 11 | 23 | 5 | 11 | 28 | 30.0 | 33.2 |
| 3 | (32) | 6 | 13 | 28 | 8 | 18 | 36 | 26.4 | 29.4 |
| 4 | (50) | 7 | 15 | 28 | 15 | 30 | 52 | 21.8 | 19.5 |
| 5 | (72) | 13 | 24 | 47 | 24 | 44 | 66 | 19.2 | 11.6 |
| 6 | (98) | 15 | 30 | 56 | 27 | 51 | 71 | 21.7 | 7.8 |

**TABLE 6. OBJECTIVE ANALYSIS USING SPHERICAL HARMONICS. M2 COMPONENT. (77 data points)**

| Degree (no. of coeff.) | | Amplitude (%) <5% | <10% | <20% | Phase (%) <5° | <10° | <20° | RMS (cm) TOTAL | DATA |
|---|---|---|---|---|---|---|---|---|---|
| 2 | (18) | 9 | 14 | 27 | 3 | 9 | 18 | 25.2 | 21.5 |
| 3 | (32) | 10 | 18 | 39 | 14 | 26 | 42 | 21.9 | 15.0 |
| 4 | (50) | 11 | 22 | 37 | 17 | 30 | 54 | 19.2 | 13.2 |
| 5 | (72) | 16 | 28 | 50 | 21 | 35 | 51 | 34.5 | 7.9 |

Tables 7 and 8 show the results obtained for the objective analysis of the K1 tide. When using the data set with 116 points the best fit to the M2 tide is obtained when estimating the coefficients corresponding to the 58 most powerful modes, this case yields a 4.2 cm RMS over the entire 462 point $\phi$ field. For the K1 tide the best fit corresponds to the case when 35 coefficients are estimated wnich yields a total RMS of 1.9 cm. For the data set containing 77 points the best fit to the M2 tide is obtained when estimating the coefficients corresponding to the 32 most powerful modes which case gives a total RMS of 8.6 cm. For this data set the best fit to the K1 tide yields a 3.3 cm total RMS by estimating 34 coefficients. The number of coefficients which yields the best fit is a function of the number of data points and their distribution in space in relation to the structure of the particular tidal component. Therefore, given a certain data set in the domain of an ocean basin, the theoretical simulation will help to choose the optimum number of functions to use in the objective analysis. Also by using the results of the objective analysis of the theoretical solution it is possible to determine the areas where additional data

**TABLE 7. COMPARISON BETWEEN OBJECTIVELY ANALYZED AND THEORETICAL FIELDS. K1 COMPONENT. (116 data points)**

| Coefficients (% of Total Power) | | Amplitude (%) <5% | <10% | <20% | Phase (%) <5° | <10° | <20° | RMS (cm) TOTAL | DATA |
|---|---|---|---|---|---|---|---|---|---|
| 20 | (72.1) | 29 | 48 | 68 | 43 | 71 | 94 | 3.4 | 3.2 |
| 35 | (83.0) | 44 | 69 | 89 | 69 | 89 | 97 | 1.9 | 1.2 |
| 40 | (85.1) | 51 | 73 | 89 | 73 | 90 | 97 | 2.1 | 1.0 |
| 50 | (88.3) | 62 | 81 | 93 | 73 | 93 | 99 | 2.2 | 0.8 |
| 70 | (92.7) | 63 | 84 | 94 | 78 | 92 | 97 | 2.2 | 0.3 |
| 100 | (96.9) | 69 | 81 | 94 | 79 | 88 | 96 | 8.1 | 0.07 |

**TABLE 8. COMPARISON BETWEEN OBJECTIVELY ANALYZED AND THEORETICAL FIELDS. K1 COMPONENT. (77 data points)**

| Coefficients (% of Total Power) | | Amplitude (%) <5% | <10% | <20% | Phase (%) <5° | <10° | <20° | RMS (cm) TOTAL | DATA |
|---|---|---|---|---|---|---|---|---|---|
| 20 | (72.1) | 24 | 42 | 66 | 42 | 66 | 90 | 4.4 | 3.7 |
| 23 | (75.3) | 26 | 45 | 70 | 44 | 73 | 89 | 3.6 | 3.5 |
| 32 | (81.6) | 40 | 61 | 81 | 54 | 78 | 94 | 5.9 | 1.1 |
| 34 | (82.6) | 39 | 62 | 81 | 53 | 79 | 94 | 3.3 | 1.0 |
| 36 | (83.5) | 40 | 66 | 83 | 57 | 79 | 96 | 3.5 | 0.8 |
| 45 | (86.8) | 50 | 72 | 89 | 66 | 83 | 95 | 6.8 | 0.5 |

measurements are most needed as shown in Figures 12 and 13. Figure 12 shows the absolute values of the differences in amplitudes between the theoretical M2 tide using 150 coefficients and the best fit using 58 coefficients and 116 data points. Figure 13 shows the corresponding values for the K1 tide when using a best fit of 35 coefficients. The numbers are rounded to the nearest digit to facilitate display. In the M2 case there are areas in the north-east Atlantic with higher than average RMS. The highest discrepancies occur at some isolated points off the coast of Labrador, Greenland, northern Australia and east Antarctica. The K1 fit shows some high values in the north-east Atlantic and the Patagonian shelf as well as in the Antarctic area in the Indian Ocean.

The results of the objective analysis of the M2 tide using spherical harmonics given in Tables 5 and 6 indicate a best fit when using an expansion of degree 5 with the 116 point data set and a best fit of degree 4 for the 77 point data set. Both cases yielded a total RMS of 19.2 cm, well above the values of 4.2 cm and 8.6 cm obtained when using the $\phi$ eigenfunctions. The K1 tide was analyzed also using spherical harmonics, the results given in Tables 9 and 10 show a best fit of 3.3 cm when using an expansion of degree 5 with the 116 point data set and a best fit of 5.9 cm when using an expansion of degree 4 with the 77 point data set.

Table 11 contains a summary and comparison between the best cases using both spherical harmonics and the eigenfunctions of the velocity potential which are referred to as Proudman functions. The Proudman functions yield better results uniformly when comparing corresponding tidal components and data sets, the improvement is more pronounced when fitting the M2 constituent which has a more complex structure. We shall point out that we have not tested every possible combination of modes when estimating the coefficients to fit the tide in the different cases. An exhaustive search might yield still better results for the Proudman functions.

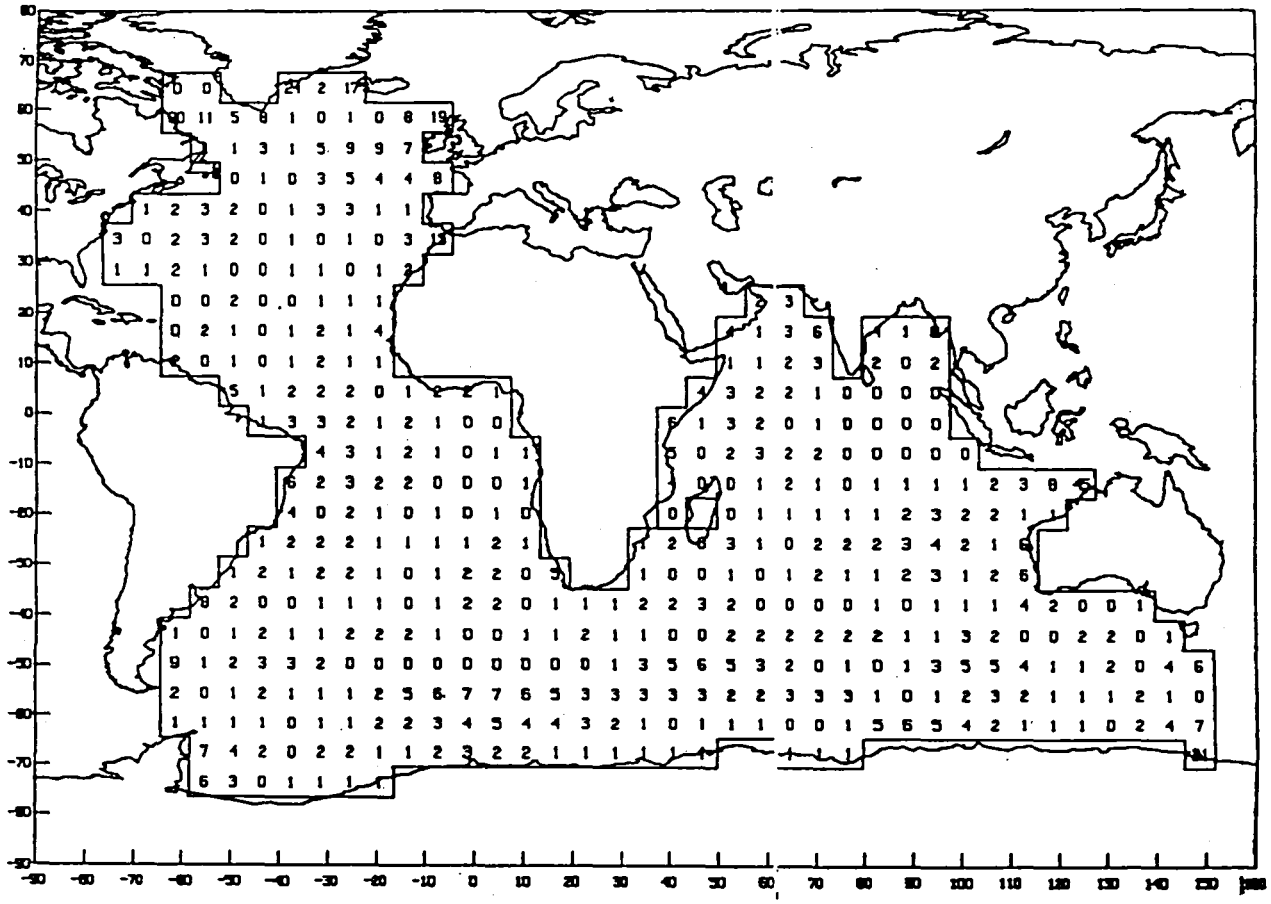

**Figure 12. M2 Tide: Amplitude Differences (cm) Between Theoretical Solution Using 150 Coefficients and 58 Coefficient Solution from 116 Point Data Set.**

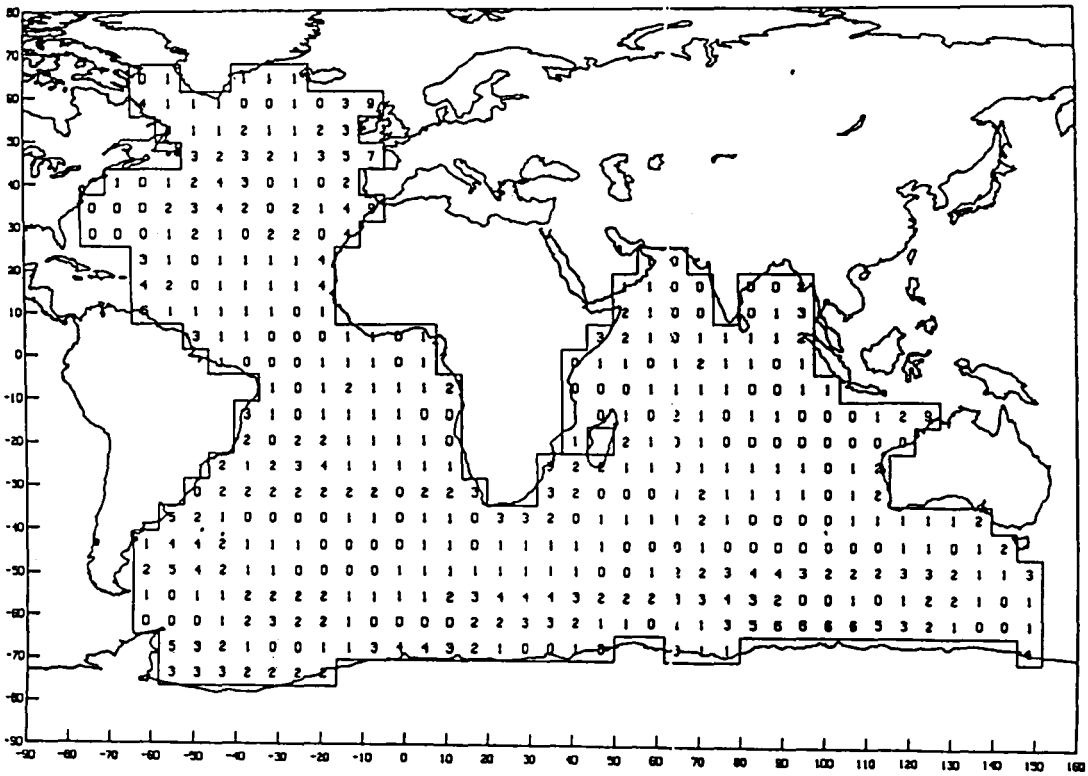

**Figure 13. K1 Tide: Amplitude Differences (cm) Between Theoretical Solution Using 150 Coefficients and 35 Coefficient Solution from 116 Point Data Set.**

**TABLE 9. OBJECTIVE ANALYSIS USING SPHERICAL HARMONICS.**
**K1 COMPONENT. (116 data points).**

| Degree | Amplitude (%) | | | Phase (%) | | | RMS (cm) | |
|---|---|---|---|---|---|---|---|---|
| (No. of Coeff.) | <5% | <10% | <20% | <5° | <10° | <20° | TOTAL | DATA |
| 2(18) | 7 | 16 | 28 | 15 | 25 | 38 | 10.1 | 9.6 |
| 3(32) | 15 | 31 | 59 | 27 | 49 | 78 | 6.4 | 6.0 |
| 4(50) | 23 | 43 | 72 | 49 | 72 | 89 | 4.1 | 3.5 |
| 5(72) | 32 | 56 | 82 | 54 | 79 | 96 | 3.3 | 2.5 |
| 6(98) | 40 | 63 | 85 | 60 | 85 | 97 | 3.4 | 1.8 |

**TABLE 10. OBJECTIVE ANALYSIS USING SPHERICAL HARMONICS.**
**K1 COMPONENT. (77 data points).**

| Degree | Amplitude (%) | | | Phase (%) | | | RMS (cm) | |
|---|---|---|---|---|---|---|---|---|
| (No. of Coeff.) | <5% | <10% | <20% | <5° | <10° | <20° | TOTAL | DATA |
| 2(18) | 7 | 16 | 33 | 9 | 19 | 37 | 10.8 | 11.4 |
| 3(32) | 13 | 29 | 52 | 22 | 43 | 70 | 6.2 | 5.6 |
| 4(50) | 19 | 43 | 70 | 39 | 66 | 90 | 5.9 | 2.6 |
| 5(72) | 24 | 45 | 70 | 39 | 63 | 87 | 10.2 | 1.8 |

TABLE 11. COMPARISON BETWEEN PROUDMAN FUNCTIONS AND SPHERICAL HARMONICS

| Tidal Component | Data Set | Method | Amplitude RMS (cm) | Amplitude RMS (% of mean value of theoretical solution) |
|---|---|---|---|---|
| M2 | 116 | Proudman functions | 4.2 | 8% |
| M2 | 116 | Spherical harmonics | 19.2 | 37% |
| M2 | 77 | Proudman functions | 8.6 | 17% |
| M2 | 77 | Spherical harmonics | 19.2 | 37% |
| K1 | 116 | Proudman functions | 1.9 | 7% |
| K1 | 116 | Spherical harmonics | 3.3 | 13% |
| K1 | 77 | Proudman functions | 3.3 | 13% |
| K1 | 77 | Spherical harmonics | 5.9 | 23% |

## 5. CONCLUSIONS

A method has been developed to objectively analyze tidal data to map the tidal components over an entire basin. The technique has been demonstrated in an application to the Lake Superior basin by Sanchez, Rao and Wolfson (1985). Now it has been applied to the Atlantic-Indian ocean basin using a 6° × 6° finite difference grid.

The computed normal modes agree fairly well with those obtained by Platzman (1975) using a different approach. The forced solutions for the M2 and K1 tidal constituents were computed also, these theoretical simulations show the same general pattern obtained by other modelers, i.e. Platzman (1984), Schwiderski (1983), Parke and Hendershott (1980) and Accad and Pekeris (1978). The theoretical solutions were obtained by including 150 eigenfunctions of the velocity potential, the resulting height and phase fields were used as data to test the objective analysis technique and as a guide in choosing the most energetic modes.

The results of the objective analysis show that it is possible to recover the M2 and K1 components with a degree of accuracy well within the error bounds of present day satellite techniques and with amplitude errors smaller than the differences existing between different numerical models in many areas of the world oceans. The Proudman functions performed consistently better than spherical harmonics in the recovery of the tides especially for the M2 constituent with its complex structure.

Future applications of the method should consider its extension to the Pacific basin, the adoption of a grid with finer resolution, the incorporation of real data from gauges and satellite measurements and the simulation and analysis of other tidal constituents. The method is especially suited for the latter since the eigenfunctions of the velocity potential and the normal modes of a particular basin are dependent only on its shape and depth and they have to be computed only once.

## References


Accad, Y., and Pekeris, C.L., 1978. "Solution of the tidal equations for the M2 and S2 tides in the world oceans from a knowledge of the tidal potential alone." *Phil Trans. Roy. Soc. London,* 290.

Cartwright, D.E., 1977. "Oceanic tides.", *Reports on Progress in Physics,* 40.

Estes, R.H., 1980. "A simulation of global ocean tide recovery using altimeter data with systematic orbit error." *Marine Geodesy,* Vol. 3, Nos. 1-4.

Hendershott, M.C., and Munk, W.H., 1970."Tides." *Ann. Rev. Fluid Mech.,* 2.

Hendershott, M.C., 1973."Ocean tides." *EOS,* Vol. 54, No. 2

Hendershott, M.C., 1977."Numerical models of ocean tides." *The Sea,* Vol. 6, Marine Modeling. Wiley-Interscience Publication.

Hendershott, M.C., 1981."Long waves and ocean tides." *Evolution of Physical Oceanography,* MIT Press.

Mazzega, P., 1985."M2 model of the global ocean tide derived from Seasat altimetry." *Marine Geodesy,* 9.

Parke, M.E., and Hendershott, M.C., 1980."M2, S2, K1 models of the global ocean tide on an elastic earth." *Marine Geodesy,* Vol. 3, Nos. 1-4.

Platzman, G.W., 1975."Normal modes of the Atlantic and Indian Oceans." *J. Phys. Oceanography,* 5.

Platzman, G.W., 1978."Normal modes of the world ocean. Part 1. Design of a finite-element barotropic model." *J. Phys. Oceanography,* 8.

Platzman, G.W., 1981."Normal modes of the world ocean. Part II: Description of modes in the period range 8 to 80 hours." *J. Phys. Oceanography,* 11.

Platzman, G.W., 1984."Normal modes of the world ocean. Part IV: Synthesis of diurnal and semidiurnal tides." *J. Phys. Oceanography,* 14.

Proudman, J., 1918."On the dynamical equations of the tides." *Proceedings of the London Mathematical Society,* 18.

Rao, D.B., 1966."Free gravitational oscillations in rotating rectangular basins." *J. Fluid Mech.,* 25.

Rao, D.B. and Schwab, D.J., 1976."Two-dimensional normal modes in arbitrary enclosed basins on a rotating earth: application to Lakes Ontario and Superior." *Phil. Trans. Roy. Soc. (London),* (A), 281.

Rao, D.B. and Schwab, D.J., 1981."A method of objective analysis for currents in a lake with application to Lake Ontario." *J. Phys. Oceanography,* 11.

Sanchez, B.V., D.B. Rao and P.G. Wolfson, 1985."Objective analysis for tides in a closed basin " *Marine Geodesy,* 9.

Schwiderski, E.W., 1979."Global ocean tides, part 11: the semidiurnal principal lunar tide (M2), Atlas of tidal charts and maps." NSWC TR 79-414.

Schwiderski, E.W., 1980."Ocean tides, Part I: global ocean tidal equations," Ocean tides, Part II: a hydrodynamical interpolation model." *Marine Geodesy,* Vol. 3, Nos. 1-4.

Schwiderski, E.W., 1981."Global ocean tides, part IV: the diurnal luni-solar declination tide (K1), Atlas of tidal charts and maps." NSWC TR 81-142.

| 1. Report No. NASA TM-87773 | 2. Government Accession No. | 3. Recipient's Catalog No. |
|---|---|---|
| 4. Title and Subtitle<br>Objective Analysis of Tidal Fields in the Atlantic and Indian Oceans | | 5. Report Date<br>June 1986<br>6. Performing Organization Code<br>621 |
| 7. Author(s) Braulio V. Sanchez, Desiraju B. Rao, and Stephen D. Steenrod | | 8. Performing Organization Report No.<br>86B0195 |
| 9. Performing Organization Name and Address<br>Geodynamics Branch, Code 621<br>Goddard Space Flight Center<br>Greenbelt, MD 20771 | | 10. Work Unit No.<br>11. Contract or Grant No.<br>13. Type of Report and Period Covered<br>Technical Memorandum |
| 12. Sponsoring Agency Name and Address<br>National Aeronautics and Space Administration<br>Washington, D.C. 20546 | | 14. Sponsoring Agency Code |

15. Supplementary Notes

Braulio V. Sanchez: Goddard Space Flight Center, Greenbelt, Maryland.
Desiraju B. Rao: National Meteorological Center, National Oceanic and Atmospheric Administration, Washington, D.C.
Stephen D. Steenrod: Applied Research Corporation, Landover, Maryland.

16. Abstract

An objective analysis technique has been developed to extrapolate tidal amplitudes and phases over entire ocean basins using existing gauge data and the altimetric measurements which are now beginning to be provided by satellite oceanography. The technique was previously tested in the Lake Superior basin by Sanchez, Rao and Wolfson (1985). The method has now been developed and applied in the Atlantic-Indian ocean basins using a 6°x6° grid to test its essential features. The functions used in the interpolation are the eigenfunctions of the velocity potential (Proudman functions) which are computed numerically from a knowledge of the basin's bottom topography, the horizontal plan form and the necessary boundary conditions. These functions are characteristic of the particular basin. The gravitational normal modes of the basin are computed as part of the investigation, they are used to obtain the theoretical forced solutions for the tidal constituents, the latter provide the simulated data for the testing of the method and serve as a guide in choosing the most energetic modes for the objective analysis. The results of the objective analysis of the M2 and K1 tidal constituents indicate the possibility of recovering the tidal signal with a degree of accuracy well within the error bounds of present day satellite techniques.

| 17. Key Words (Selected by Author(s)) | 18. Distribution Statement |
|---|---|
| Objective analysis, tidal fields, normal modes, M2, K1, Atlantic, Indian, ocean basins | Unclassified - Unlimited<br>Subject Category 48 |

| 19. Security Classif. (of this report) | 20. Security Classif. (of this page) | 21. No. of Pages | 22. Price* |
|---|---|---|---|
| Unclassified | Unclassified | 24 | A02 |

*For sale by the National Technical Information Service, Springfield, Virginia



GSFC 25-44 (10/77)

NASA-Langley, 1986

End of Document